ResearchGate

See discussions, stats, and author profiles for this publication at: https://www.researchgate.net/publication/320741361

Heat evolution from silica-supported nano-composite samples under exposure to hydrogen isotope gas

Conference Paper · November 2017

CITATIONS
0

17 authors, including:

Akito Takahashi
Technova Inc
264 PUBLICATIONS **1,186** CITATIONS

SEE PROFILE

Some of the authors of this publication are also working on these related projects:

Leading the Japanese Gvt NEDO project on anomalous heat effect of nano-metal and hydrogen gas interaction View project

Nuclear Data and Neutronics for DT Fusion Reactors View project

All content following this page was uploaded by Akito Takahashi on 01 November 2017.

The user has requested enhancement of the downloaded file.

Heat evolution from silica-supported nano-composite samples under exposure to hydrogen isotope gas

Akira Kitamura[1,5], Akito Takahashi[1], Koh Takahashi[1], Reiko Seto[1], Takeshi Hatano[1],
Yasuhiro Iwamura[2], Takehiko Itoh[2], Jirohta Kasagi[2],
Masanori Nakamura[3], Masanobu Uchimura[3], Hidekazu Takahashi[3], Shunsuke Sumitomo[3],
Tatsumi Hioki[4], Tomoyoshi Motohiro[4], Yuichi Furuyama[5],
Masahiro Kishida[6], Hideki Matsune[6]

[1] Technova Inc., 100-0011 Japan,
[2] Research Center for Electron Photon Science, Tohoku University, 982-0826 Japan,
[3] Research Division, Nissan Motor Co., Ltd., 237-8523 Japan,
[4] Green Mobility Research Institute, Institutes of Innovation for Future Society,
Nagoya University, 464-8603 Japan,
[5] Graduate School of Maritime Sciences, Kobe University, 658-0022 Japan,
[6] Graduate School of Engineering, Kyushu University, 819-0395 Japan

E-mail: kitamuraakira3@gmail.com

Abstract Hydrogen isotope absorption characteristics of nanoparticles supported by silica, Pd/SiO_2 ("PSf1") and $CuNi_{10}/SiO_2$ ("CNS3"), have been examined. Large absorption energy (1.3±0.3 eV/Pd) with large apparent loading ratio (L_M = 2.6) was observed in the initial phase of the D-PSf1#1 run with D_2 at room temperature, which could be ascribed to reduction of PdO and hydrogen absorption by Pd nanoparticles. To reduce the NiO in the CNS3 sample, heating up to around 200 °C was necessary. The excess heat was observed in the elevated temperature phases of the runs with CNS3, while no excess heat was observed with PSf1. Taking also into account the experimental results obtained previously for other samples, we can conclude that the excess heat is observed only in the elevated temperature phases of the runs with binary nanocomposite samples, but not with single-element nanoparticles. In the H-CNS3#2 run, the excess heat amounts to 200 eV/Ni or more than 0.9 keV/H without detectable dose rate of hard radiations, which cannot be explained by any chemical process.

Index Terms – Silica supported nanoparticles, $Cu{\cdot}Ni/SiO_2$, Pd/SiO_2, hydrogen gas absorption, excess power, 200 eV/Ni, 0.9 keV/H.

I. INTRODUCTION

There have been increasing interests in experiments of hydrogen-gas charged nickel-based nano-composite samples for excess power generation, owing to higher availability of nickel than palladium. A Ni·Cu·Mn alloy thin wire, for example, has been examined extensively by Celani et al. [1]. In addition, a number of entrepreneurs are publicizing their own "products" of nano-fabricated samples on web sites with undisclosed details, and therefore with little scientific corroboration [e.g., 2 – 3]. Among them, replication experiments of the Rossi-type reactors have been performed by several researchers [4 – 7], which seemingly appears to show unignorable reproducibility of the Rossi method. However, little is known about the accuracy of the calorimetry and the mechanism of the claimed anomalously large energy production.

As reviewed in ref. [8], the 8 year-long (2008-2015) series of study on anomalous heat effects by interaction of metal nanoparticles and D(H)-gas under the collaboration of Technova Inc. and Kobe University has become the basis for the present collaborative research of a new CO_2 free energy source. This new project on New Metal-Hydrogen Energy was started on October 2015 under the collaboration of six Japanese organizations, one of which the individual author of the present paper belongs to. The first report of the results by the project was done in ICCF20 [9].

In the present work, hydrogen isotope absorption by nickel-based silica-supported nanocomposite samples has been examined as the collaborative work using the experimental apparatus installed at Kobe University [8 - 13]. The system has a reaction chamber containing the sample with a capacity of 500 cc, and a flow-calorimetry system capable of working at elevated temperatures up to 300 °C with use of a liquid hydrocarbon coolant. The samples tested so far include silica-included Pd nanoparticles ("PSf1") fabricated in Kyushu University and mesoporous-silica-supported $CuNi_{10}$ nanoparticles ("CNS3") synthesized in Kobe University, whose D(H)-absorption/heat-generation characteristics are discussed in the present paper.

II. EXPERIMENTAL PROCEDURE AND SAMPLES

The PSf1 sample consists of Pd nanoparticles embedded in silica balls with diameter of several tens of nm. The detailed description of this sample will be published elsewhere. The CNS3 sample consists of $CuNi_{10}$ nanoparticles supported by the mesoporous silica (mp-silica) PC700G fabricated by Admatechs Co. Ltd. The sample was synthesized from a solution of nickel chloride and copper chloride containing the mp-silica powder as a suspended material to adsorb Ni and Cu in mesoscopic pores. After filtration, the mp-silica was annealed at 800 °C for 3 hrs. Each sample containing 8.4-g-Pd (PSf1) or 1.2-g-Cu and 11.4-g-Ni (CNS3) occupied the 500-cc volume of the reaction chamber (RC) without any filler.

The specifications of the samples are tabulated in Table 1. Those of the similar sample CNS2 [11,12] are also shown in the figure for comparison. The particle size was visually observed in STEM-EDS photos. In the case of the CNS samples, the diameter of the Ni and Cu particles are in the range of 5 ~ 100 nm. It seems that the larger diameter particles are sticking on the outer surface of the mp-silica blocks. The Ni and Cu atoms appear to be included in the same pores of the mp-silica, or contained in the larger diameter particles with a density ratio approximately equal to the mixing ratio.

Table 1. Specifications of the samples tested.

	Silica-coated Pd nanoparticle; PSf1		Mesoporous-silica-supported CuNi nanoparticle; CNS3		Mesoporous-silica-supported CuNi; CNS2 (for reference)	
Particle size	20.8 nm (average)		10 ~ 100 nm		5 ~ 20 nm	
Fabricated at;	Kyushu Univ.		Technova-Kobe U.		Technova-Kobe U.	
Tested on;	Sept. – November 2016		Nov. 2016 – Feb. 2017		Aug. – Oct. 2014	
	Mass (g)	Number of moles	Mass (g)	Number of moles	Mass (g)	Number of moles
Amount	115.37	---	150.50	---	160.33	---
O	1.27	0.079	3.40	0.21	3.76	0.24
Ni	---	---	11.36	0.19	12.07	0.21
Cu	---	---	1.22	0.02	1.89	0.03
Pd	8.42	0.079	---	---	---	---
Zr	---	---	---	---	---	---
SiO_2	105.68	1.76	134.52	2.24	146.38	2.44

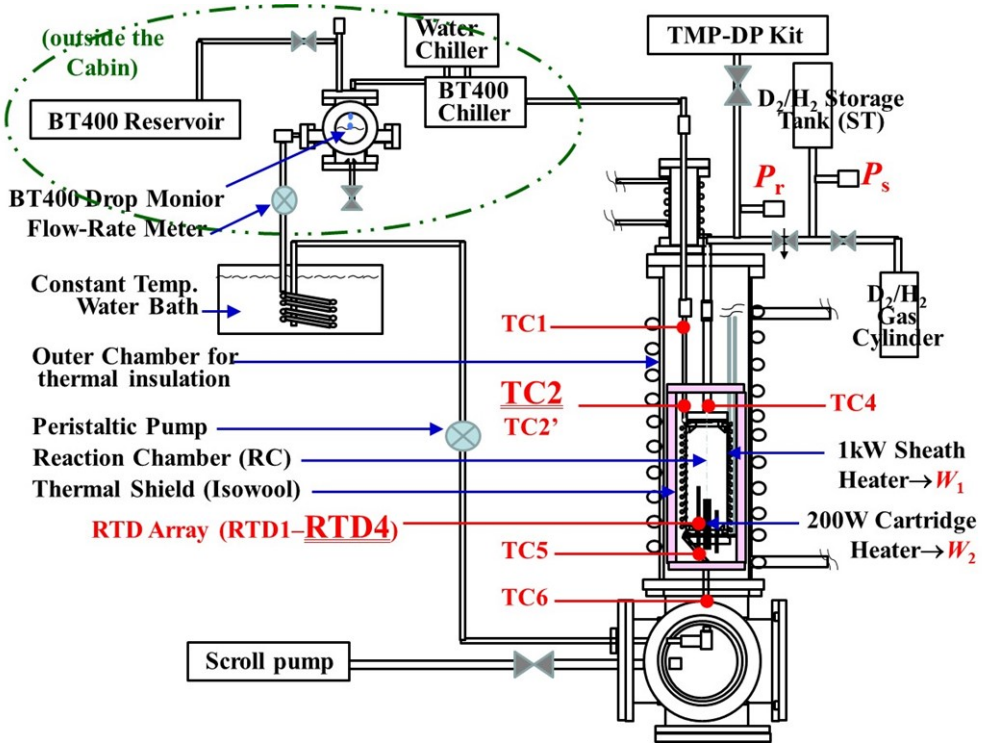

Fig. 1. Schematic of C_1 absorption system equipped with oil-flow-calorimeter system with flow-rate-monitors and dual heaters.

A schematic of the absorption-calorimetry system C_1 is shown in Fig. 1. Refer to the references [9, 11 - 13] for detailed description of the system. Calibration of the flow calorimetry with a flow rate of 20 cc/min was performed using the bare mp-silica powder. The heat conversion coefficient from the power to the oil-outlet temperature T_{C2} at TC2, dT_{C2}/dW = 1.65 °C/W or 1.16 °C/W, was obtained at room temperature (R.T.) or in the temperature range from 200 – 300 °C, respectively. The heat recovery rate, 0.88 – 0.79 in the same temperature range, was calculated by

$$R_h = F^{\alpha}\cdot\rho\cdot C\cdot(T_{C2}-T_{C6})/(W_1+W_2), \quad (1)$$

where F, ρ and C are the flow rate, the mass density and the specific heat capacity, respectively, of the coolant BarrelTherm-400 (BT400), Matsumura Oil Co. Ltd., and W_1 and W_2 the power of the outer sheath heater (#1) and the inner cartridge heater (#2), respectively. The parameter α is determined empirically as follows. A correction factor for the flow rate fluctuation ΔF (= $F - F_0$) to be subtracted from T_{C2} is derived from eq. (1);

$$\Delta T_{C2} = (dT_{C2}/dF)\cdot\Delta F = (-\Delta F/F)\cdot(W_1+W_2)\cdot(dT_{C2}/dW)\cdot\alpha. \quad (2)$$

The correction is applied to T_{C2} for some samples or gas species to determine α, so that the corrected temperature is not unreasonable, not giving negative excess temperature, or giving null excess for the Ar filling run, in the flow rate range of $0.825 \le F/F_0 \le 1$ for F_0 = 20 cc/min;

$$\alpha = 1.9\times10^{-2}\cdot\exp[4.0\cdot(F/F_0)]. \quad (3)$$

The calibration run also serves as a control run giving reference temperatures, the flow rate of BT400 and the heater power for foreground runs using the silica-supported samples. Comparing the temperatures in the foreground and background runs, the excess power will be calculated using the heat conversion coefficient mentioned above.

III. RESULTS AND DISCUSSION

(1) PSf1 SAMPLE

Deuterium (D) absorption runs, D-PSf1#1, #2, #3 and #4, were performed after vacuum baking (#0) for more than 30 hours at RTD and TC2 temperatures of 200 - 300 °C with the heater power of (W_1+W_2) = (69+20) ~ (124+30) W and with the BT400 flow rate of 20 cc/min. The temperature history in the D-PSf#0 through #4 is shown in Fig. 2(a). Each time the heater power was varied, the phase number is advanced; #1-1 for D_2 introduction with the heater power of (0+0) W, #1-2 for (20+10) W, #1-3 for (30+20) W, and so on. At the end of each run, the heated sample was outgassed ("OG" phase) by evacuating the RC, and the run number is advanced for the succeeding run started with filling of the fresh D_2 gas.

In fig. 2(b) are shown the pressures at the RC and at the storage tank (ST), P_r and P_s, respectively, and the apparent loading ratio $L_M \equiv$ (D/M) or (H/M), *i.e.*, the number of hydrogen isotope atoms lost from the gas phase relative to the number of metal atoms (Pd in PSf1 runs or Ni in CNS3 runs). The loading ratio is calculated from the values of P_r and P_s, and volumes of the RC and the ST with a correction for the temperature based on the Boyle-Charles' law using the averaged temperature of four RTD's.

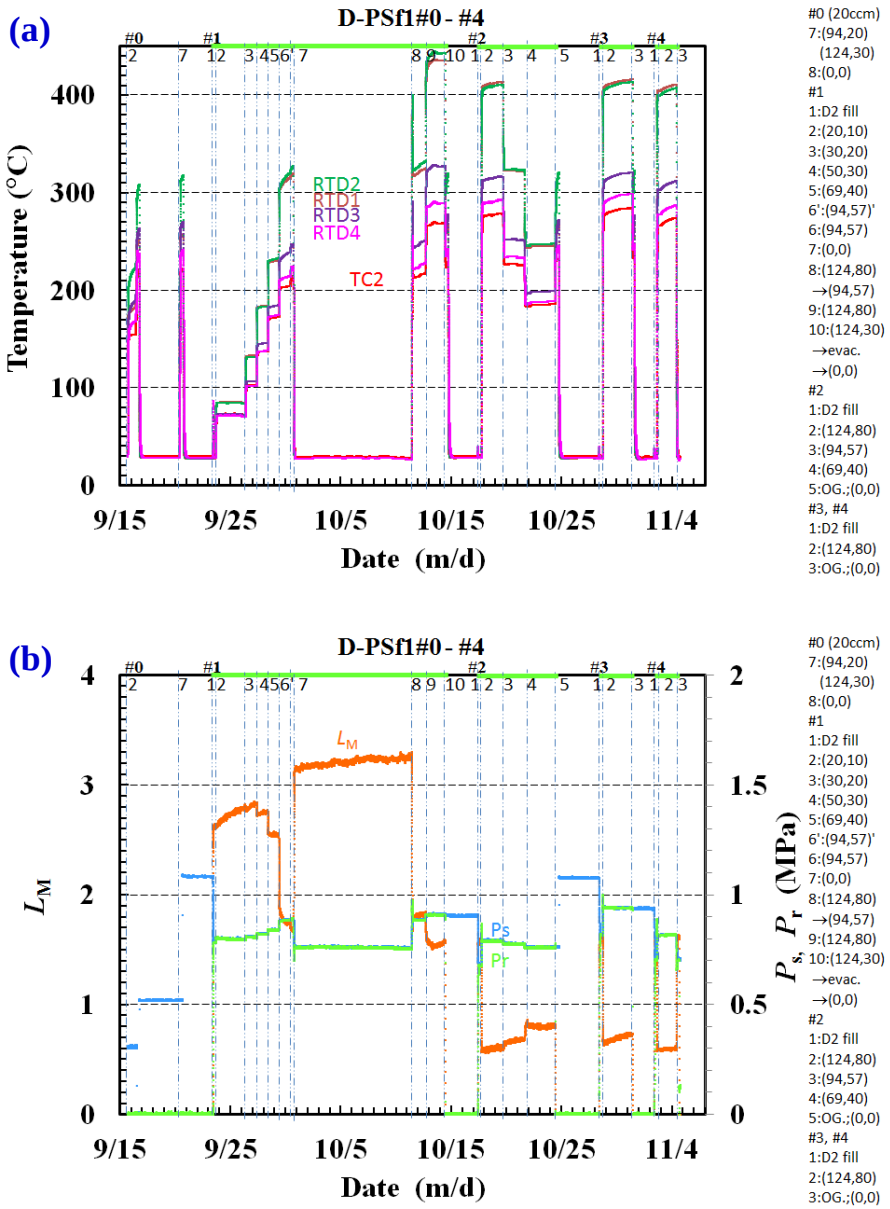

Fig. 2. Temperature (a) and D loading (b) history in D-PSf1#0 through #4 runs.

It should be noted that the apparent loading ratio L_M is very high in the low temperature phases of the #1 run (#1-1 through #1-4, where RTD and TC2 temperatures are below 200 °C), while it is modest in the #2 run and later. It is inferred that the PdO molecules in the virgin sample are reduced by D_2 introduction in the #1-1 phase, and the D_2O molecules are exhausted in the evacuation process in the #1-10 OG phase. The L_M in the #2 - #4 runs is the proper loading ratio reflecting the proper temperature dependence, and is very reproducible.

(1-1) Absorption and heat evolution at R.T.

The initial bursts of heat are observed on the RTD and TC traces at the beginning of the #1-1 phase at R.T. Figure 3 shows the thermal power calculated from the temperature evolution in the #1-1 phase with the conversion factor mentioned above.

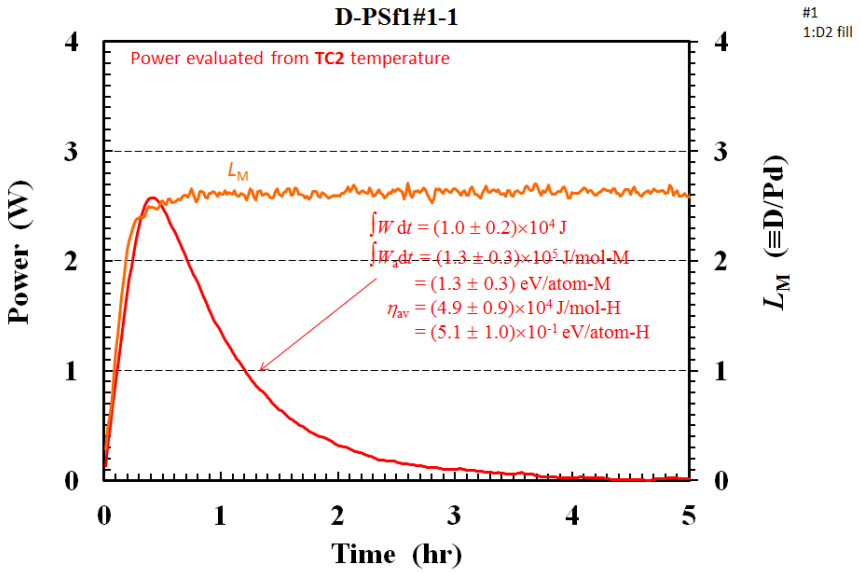

Fig. 3. Thermal power and deuterium loading ratio in the room temperature phase of the virgin sample run, D-PSf1#1-1.

The hump at TC2 is time-integrated to calculate an emerging energy per an absorbent atom,

$$E_a = \int_0^t W_a \, dt, \tag{2}$$

where W_a is the power per an adsorbent atom, Pd in the present case. The energy E_a is calculated to be 1.3 ± 0.3 eV/atom-Pd. This is rather large in view of the hydrogen absorption energy of about 0.2 eV/atom-Pd for bulk crystalline Pd. The energy E_a is divided by L_M to obtain the specific energy per D atom adsorbed/absorbed or lost from the gas phase, $\eta_{av} \equiv E_a/L_M$, averaged over the #1-1 phase. Similarly, E_a and η_{av} are calculated for #*n*-1, where *n* is the integer indicating the run number. Those are summarized in Fig. 4 together with L_M.

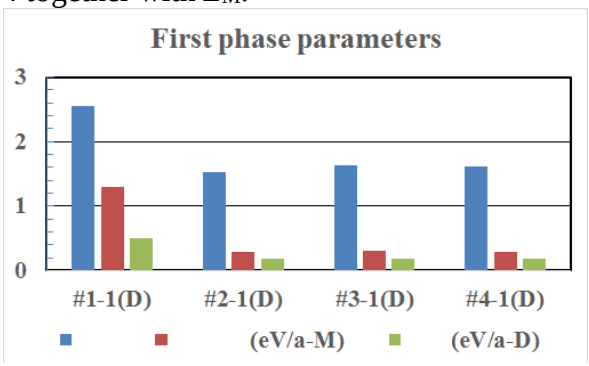

		#1-1(D)	#2-1(D)	#3-1(D)	#4-1(D)
L_M		2.55	1.53	1.63	1.61
E_a (≡$\int W_a dt$)	(eV/a-M)	1.30	0.29	0.31	0.29
η_{av}	(eV/a-D)	0.51	0.19	0.19	0.18

Fig. 4. Comparison of loading ratio and specific output energies in room temperature phases of D-PSf1#*n*-1 runs.

The reproducibilities of not only L_M but also E_a and η_{av} are rather good for the runs #*n*-1 ($n > 1$). This means that the reduction of PdO was completed in #1-1, and that the values of L_M, E_a and η_{av} in #*n*-1 ($n > 1$) are the intrinsic ones for the sample. As one of the nanoparticle characteristics, the intrinsic $L_M \sim 1.6$ is larger than that for the bulk Pd ~ 0.8, while η_{av} is nearly equal to that (~ 0.2 eV/a-D) for the bulk Pd.

Now the large values in #1-1 are examined to check whether any reaction is involved other than reduction of PdO and adsorption/absorption. If we assume that (100·*y*)% of Pd atoms were oxidized in the virgin sample, we have the following set of energy equations;

$$(PdO + D_2 \rightarrow Pd + D_2O + 1.77 \text{ eV/atom-Pd})\cdot\boldsymbol{y}, \quad (3)$$

$$Pd + (\boldsymbol{x}/2)D_2 \rightarrow PdD_x + 0.19\cdot\boldsymbol{x} \text{ eV/atom-Pd}. \quad (4)$$

Doing addition of these two, we obtain

$$\boldsymbol{y}\cdot PdO + \{(2\cdot\boldsymbol{y}+\boldsymbol{x})/2\}D_2 \rightarrow PdD_x + \boldsymbol{y}\cdot D_2O + (1.77\cdot\boldsymbol{y} + 0.19\cdot\boldsymbol{x}) \text{ eV/atom-Pd}. \quad (5)$$

The amount of the product D_2O is $\boldsymbol{y}\cdot$79 mmol, since we have 79 mmol of Pd. Almost all of them turn into the liquid phase, since only 0.8 mmol is necessary to fill the free space of 450 cc of the RC at the saturated H_2O vapor pressure of 4 kPa. Then the apparent D/Pd = $(2\cdot y+x) = 2.6$. And if $x = 1.6$ observed in the #*n*-1 ($n \geq 1$) phases apply also to the #1-1 phase, then $y = 0.5$. The reaction energy reduces to $E_a = (1.77\cdot\boldsymbol{y}+0.19\cdot\boldsymbol{x}) = 1.2$ eV/a-Pd, and therefore $\eta_{av} = 0.46$ eV/a-D. These are in fairly good agreement with the observed values of E_a and η_{av}. Thus, by assuming that the Pd was partially oxidized with a fraction of 0.5 in the virgin sample, the observed energies could be reasonably accounted for without assuming unconventional reactions including nuclear one.

(1-2) Heat evolution at E.T.

Next, we discuss the oil-outlet temperature T_{C2} in the elevated temperature phases in the D-PSf1 runs, T_{C2}(PSf1) (the red line in Fig. 5), in comparison with $T_{C2}(SiO_2)$ in the calibration / control run using the mp-silica (the black line in Fig. 5). As is seen, T_{C2}(PSf1) is higher or lower than $T_{C2}(SiO_2)$ even by more than 10 °C in some elevated temperature phases. This is largely due to fluctuation of the flow rate. When we apply the correction for the flow rate fluctuation according to eq. (2), the difference between them is reduced to below 2 ~ 3 °C.

The difference is converted to power by dividing it by dT_{C2}/dW, and shown in Fig. 6. We conclude that the PSf1 sample containing single-element nanoparticles shows no anomaly in the elevated temperature range up to 300 °C at TC2, if we admit a systematic error of ±2.3 W, which is ±1.2% of the input power of 204 W.

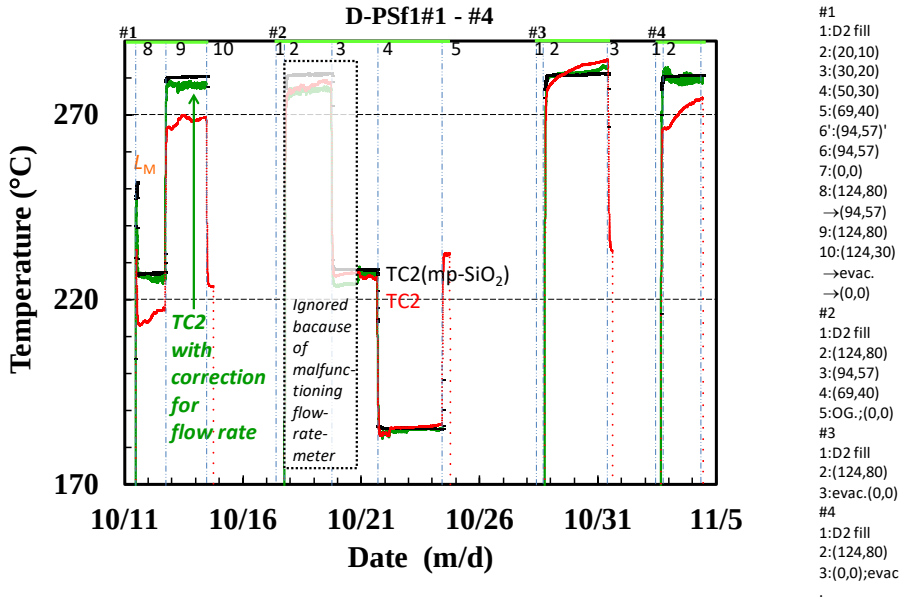

Fig. 5. Excess temperature in elevated temperature phases of D-PSf1#1 through #4 runs.

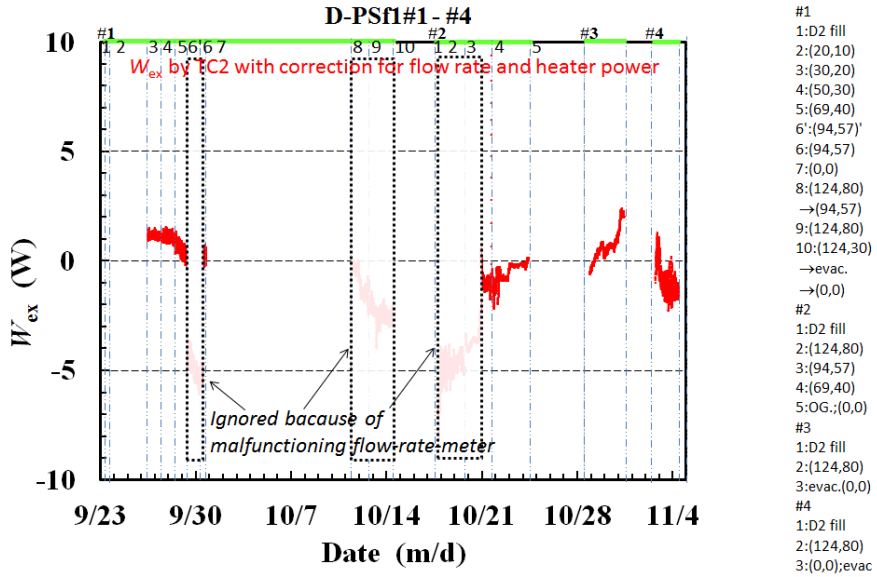

Fig. 6. Excess power in elevated temperature phases of D-PSf1#1 through #4 runs.

(2) CNS3 SAMPLE

Protium absorption runs, H-CNS3#1 and #2, were performed similarly. The temperatures at TC2 and RTD1 ~ RTD4 are shown in Fig. 7(a), and the H loading ratio L_M together with the pressures at ST and RC are shown in Fig. 7(b). In contrast to PSf1 sample, little absorption is observed in the R.T. phases, #1-1 and #2-1, while substantial consumption of H_2 is observed in the elevated temperature phases.

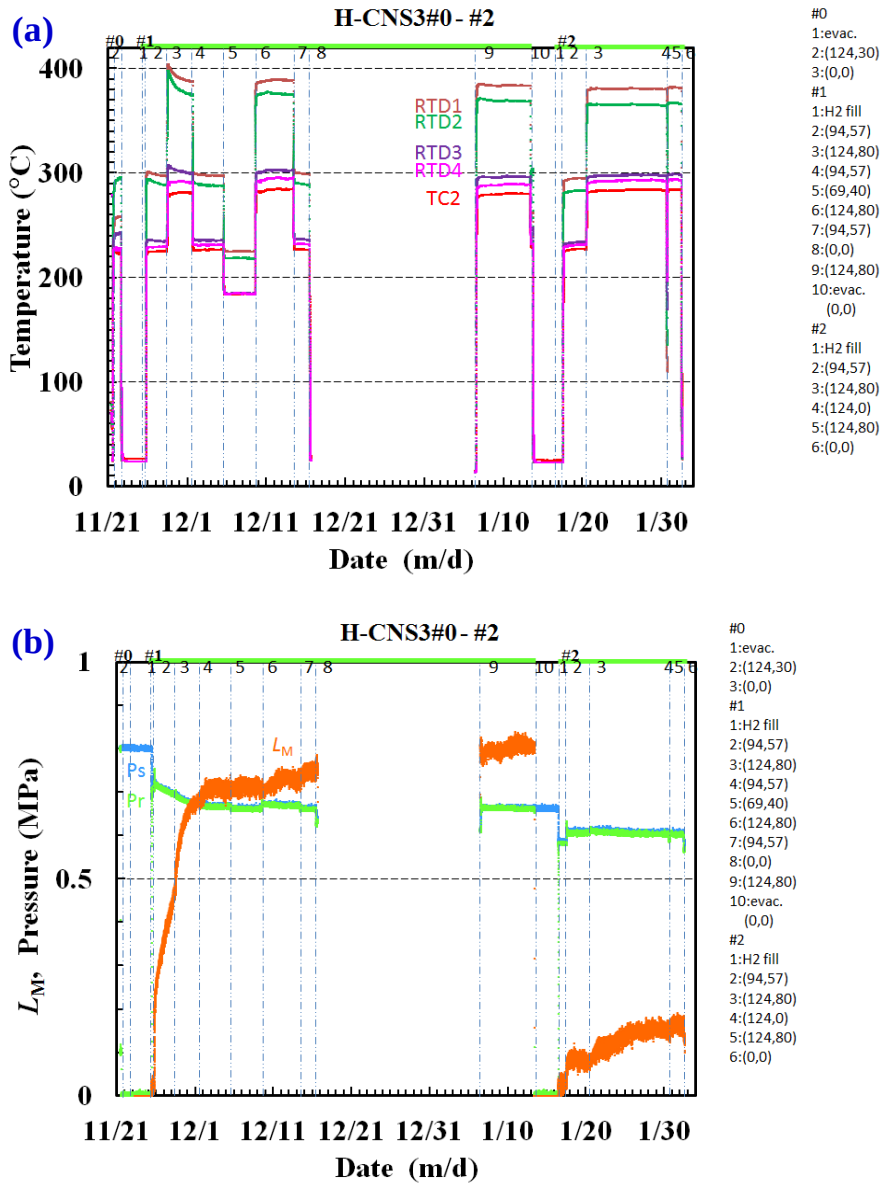

Fig. 7. Temperature (a) and H loading (b) history in H-CNS3#1 and #2 runs.

The temperature evolution in the #1-1 phase at R.T. is shown in Fig. 8. The apparent loading ratio L_M is small, and the initial burst of heat is not substantial, in accordance with the established fact that both Ni and Cu particles do not absorb much hydrogen isotopes at R.T. in contrast to Pd. The first-phase energy evaluated from T_{C2}, E_a = $(1.6\pm0.8)\times10^{-2}$ eV/atom-M, is more than one-order-of-magnitude smaller than that in the D-PSf1#1-1 phase. However, the resultant specific absorption energy is not so small; $\eta_{av} = (6.5\pm3.2)\times10^{-1}$ eV/atom-H.

The apparent loading ratio L_M increases up to about 0.8 at elevated temperatures above ~ 200 °C in #1-2 and later phases. However, it does not have large values any more in the #2 run. Similar tendency had been observed also for the PNZ3 and CNZ5 samples [9]. These phenomena are consistent with a view that the main reaction consuming H_2 is deoxidation occurring at elevated temperatures;

$$NiO + D_2(H_2) \rightarrow Ni + D_2O(H_2O) + 0.176\ (0.033)\ eV/atom\text{-}Ni, \quad (6)$$
$$CuO + D_2(H_2) \rightarrow Cu + D_2O(H_2O) + 1.00\ (0.86)\ eV/atom\text{-}Cu. \quad (7)$$

The very small value of L_M at R.T. in the #1-1 phase is simply a result of Arrhenius law for absorption with an activation energy of around 0.04 eV as inferred by the temperature dependence of the absorption [9].

Since heating by external power is necessary to induce the reaction (6) and (7) thoroughly, it is very difficult to distinguish the reaction energy from the heater power. Therefore it is difficult to make similar discussion to that for the PSf1 sample using eqs. (3) – (5).

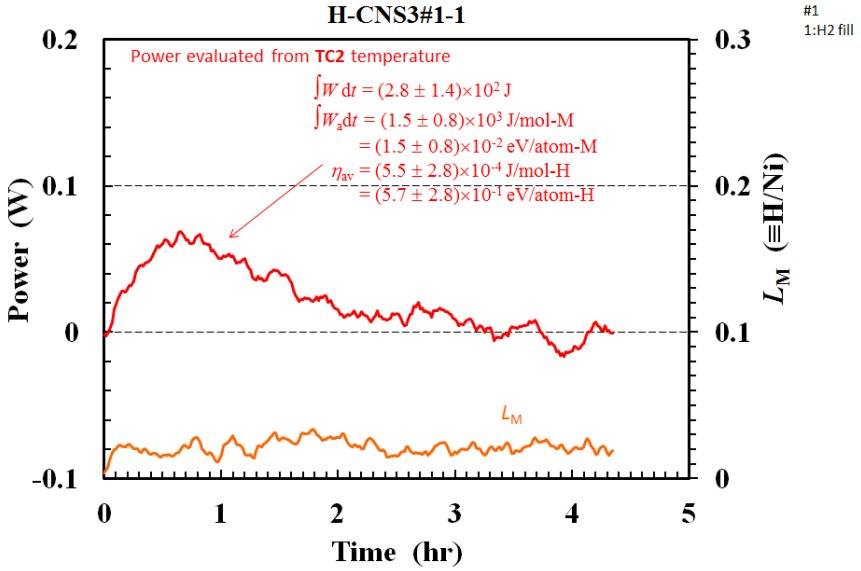

Fig. 8. Thermal power and protium loading ratio in room temperature phase of H-CNS3#1-1.

Next, we discuss the excess power in the elevated temperature phases in the H-CNS3 runs. The temperature difference was converted to the excess power, after correction for the input heater power and the flow rate of BT400 as described above, and shown in Fig. 9. When we take into account the systematic error decided above, we see that in the CNS3 powder some anomalous effect is induced to generate excess power in some phases with the elevated temperature of about 200 to 300 °C at TC2.

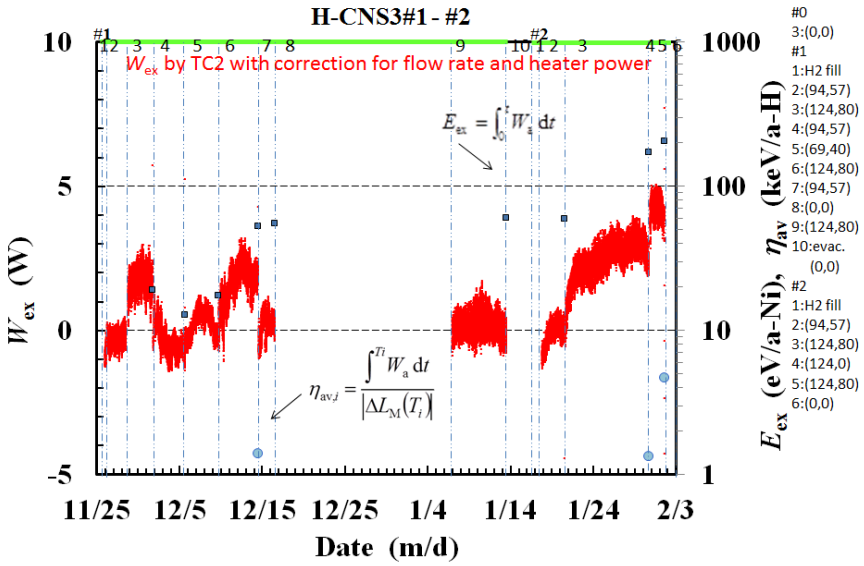

Fig. 9. Excess power in elevated temperature phases of H-CNS3#1 and #2 runs.

The phase-averaged sorption energy $\eta_{av,i}$ (closed circles) and the integrated excess energy E_a (closed squares) in the elevated temperature phases are also plotted in Fig. 9. It should be noted that $\eta_{av,i}$ is defined as E_a divided by the absolute value of ΔL_M, the increment of adsorbed/absorbed hydrogen atoms in the relevant phase;

$$\eta_{av;i} \equiv \frac{\int_0^{T_i} W_a \, dt}{|\Delta L_M(T_i)|}, \tag{8}$$

The absolute value is taken to keep $\eta_{av,i}$ positive under desorption. This is because we assume that the exothermic event could occur along with hydrogen isotope displacement under both absorption and desorption. The value of $\eta_{av,i}$ approaches 5 keV/H, and the integrated output energy E_a exceeds 200 eV/Ni. However, the definition of $\eta_{av,i}$ is rather problematic, since the real number of the hydrogen atoms getting in and out of the surfaces of the nanoparticles is not always represented by $|\Delta L_M|$ in the denominator of eq. (8). Even if we divide E_a by the total amount of H absorbed in each run, L_M, to evaluate the integrated output energy per an H atom participating in the absorption, the energy is far beyond the value explainable by any chemical reaction; E_a/L_M = 0.9 keV/H in the H-CNS3#2 run. The large values of the excess energy suggest the nuclear origin of the excess heat.

The excess power is observed, but with marginal amplitude in view of the systematic error of ±2.3 W. We compare the present result with that for the CNS2 sample having the similar composition, $CuNi_7$/mp-silica [11,12]. The result is reproduced in Fig. 10. The excess power exceeding 10 W for the CNS2 is much larger than for the CNS3 discussed above. The phase-averaged sorption energy $\eta_{av,i}$ ~ 20 keV/a-H and the integrated excess energy E_a = 700 eV/a-Ni are accordingly much larger than for the CNS3. Further examination is necessary to conclude that this difference is caused by the difference in the composition.

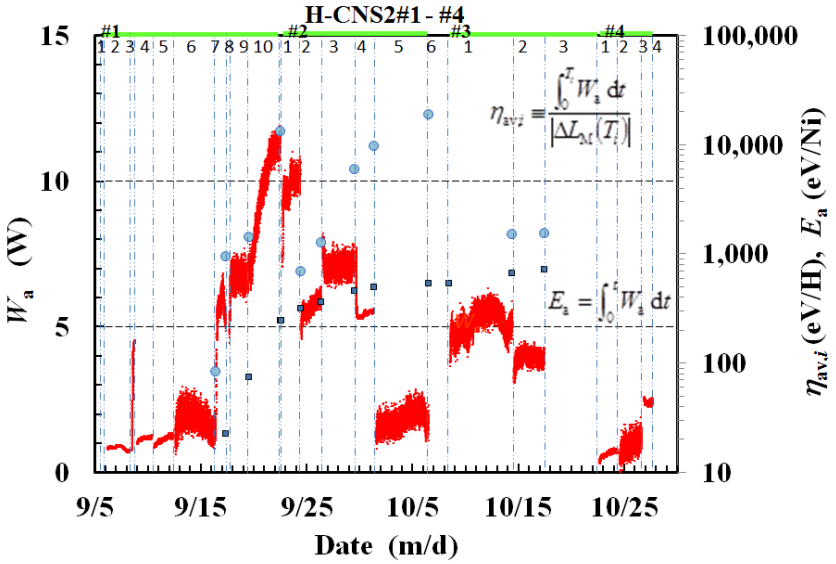

Fig. 10. Excess power in elevated temperature phases of H-CNS2#1 through #4 runs [11,12] reprinted for reference.

Finally, the result of measurements of γ-ray counting rate and neutron dose rate is shown in Fig. 11. There are some periods with high neutron dose rate. However, they agree with the periods when the accelerator in the next room was operated in the neutron emitting mode. We conclude that any hard radiation does not accompany the excess heat at least of the order of several W.

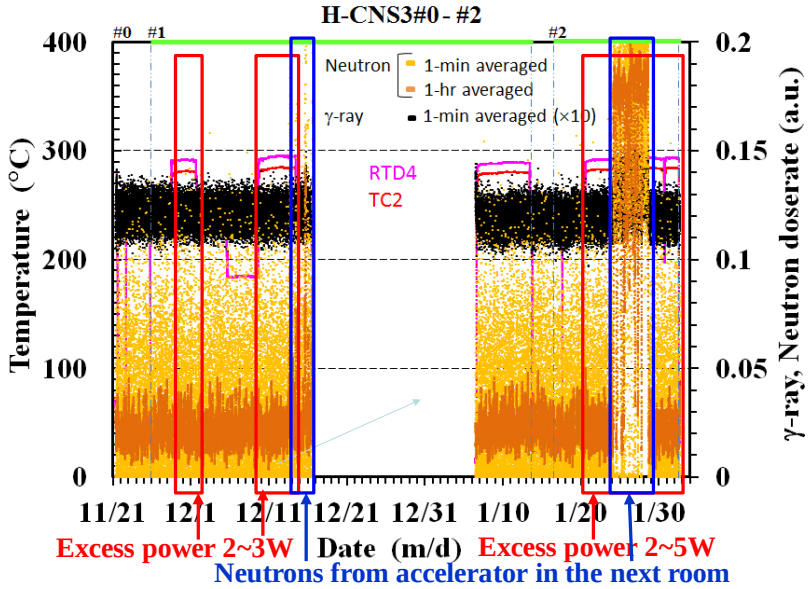

Fig. 11. Radiations and temperatures at TC2 and RTD4 in H-CNS3 runs.

IV. SUMMARY AND CONCLUDING REMARKS

The results of the absorption/heat measurements are summarized as follows in comparison with those obtained previously for other samples:

(1) It is not impossible to ascribe hydrogen absorption and heat evolution in the initial phase at R.T. to reduction of PdO and hydrogen absorption by Pd nanoparticles in the PSf1 sample.
(2) Heating up to around 200 °C is necessary to reduce the NiO in the CNS3 sample.
(3) In the E.T. phases, the excess heat is observed in the runs with binary nanocomposite samples (CNS3 in the present work), while no excess heat is observed with single-element nanoparticles (PSf1 in the present work).
(4) In the CNS3#2 run, the excess heat amounts to 200 eV/Ni (20 MJ/mol) or more than 0.9 keV/H (90 MJ/mol) without detectable dose rate of hard radiations, which cannot be explained by any chemical process.

References

[1] F. Celani, E. F. Marano, B. Ortenzi, S. Pella, S. Bartalucci, F. Micciulla, S. Bellucci, A. Spallone, A. Nuvoli, E. Purchi, M. Nakamura, E. Righi, G. Trenta, G. L. Zangari, and A. Ovidi, "Cu-Ni-Mn alloy wires, with improved sub-micrometric surfaces, used as LENR device by new transparent, dissipation-type, calorimeter", J. Condensed Matter Nucl. Sci. **13** (2014) 56-67.

[2] F. Piantelli / Nichenergy; http://e-catsite.com/2012/06/15/piantelli-moves-closer-to-commercialization/.

[3] A. Rossi / Leonardo Corporation; http://ecat.com/.

[4] G. Levi, E. Foschi, B. Höistad, R. Pettersson, L. Tegner and H. Essen., http://www.sifferkoll.se/sifferkoll/wp-content/uploads/2014/10/LuganoReportSubmit.pdf.

[5] A. G. Parkhomov, International Journal of Unconventinal Science, **6**(2) (2014) 57-61; ibid. **7**(3) (2015) 68-72; ibid. **8**(3) (2015) 34-39.

[6] S. Jiang, http://ja.scribd.com/doc/267085905/New-Result-on-Anomalous-Heat-Production-in-Hydrogen-loaded-Metals-at-High-Temperature, (2015).

[7] J. Cole, http://www.lenr-coldfusion.com/2015/04/16/experiment-generates-apparent-excess-heat/, (2015).

[8] A. Takahashi, A. Kitamura, K. Takahashi, R. Seto, T. Yokose, A. Taniike and Y. Furuyama, "Anomalous Heat Effects by Interaction of Nano-metals and D(H)-gas", Proc. ICCF20, pp.13-24 (2016), Tohoku University.

[9] Akira Kitamura, Akito Takahashi, Koh Takahashi, Reiko Seto, Yuki Matsuda,Yasuhiro Iwamura, Takehiko Itoh, Jirohta Kasagi,Masanori Nakamura, Masanobu Uchimura, Hidekazu Takahashi,Tatsumi Hioki, Tomoyoshi Motohiro, Yuichi Furuyama, Masahiro Kishida, "Collaborative Examination on Anomalous Heat Effect Using Nickel-Based Binary Nanocomposites Supported by Zirconia", to be published in J. Condensed Matter Nucl. Sci. (Proc. ICCF20, pp.93-104 (2016)).

[10] A. Kitamura, A. Takahashi, R. Seto, Y. Fujita, A. Taniike and Y. Furuyama, "Brief summary of latest experimental results with a mass-flow calorimetry system for anomalous heat effect of nano-composite metals under D(H)-gas charging", Current Science, **108**(4) (2015) 589-593.

[11] A. Kitamura, A. Takahashi, R. Seto, Y. Fujita, A. Taniike and Y. Furuyama, "Comparison of some Ni-based nano-composite samples with respect to excess heat evolution under exposure to hydrogen isotope gases", Proc. JCF15 (2015) 1-19.

[12] A. Kitamura, A. Takahashi, R. Seto, Y. Fujita, A. Taniike, Y. Furuyama, “Effect of Minority Atoms of Binary Ni-Based Nano-Composites on Anomalous Heat Evolution under Hydrogen Absorption”, J. Condensed Matter Nucl. Sci. **19** (2016) 135-144 (Proc. ICCF19 (2015)).
[13] A. Kitamura, E. F. Marano, A. Takahashi, R. Seto, T. Yokose, A. Taniike and Y. Furuyama, “Heat evolution from zirconia-supported Ni-based nano-composite samples under exposure to hydrogen isotope gas”, Proc. JCF16 (2016) 1-16

View publication stats